Supporting information for

Anodic SnO_2 Porous Nanostructures with Rich Grain Boundaries for Efficient CO_2 Electroreduction to Formate

Ruizhen Ma,[b] Yan-Li Chen,[a] Yongli Shen,[b] Heng Wang,[a] Wei Zhang,[a,*] Su-Seng Pang,[c] Jianfeng Huang,[d,*] Yu Han,[e] Yunfeng Zhao,[b,*]

[a] State Key Laboratory of Quality Research in Chinese Medicine, Macau Institute for Applied Research in Medicine and Health, Macau University of Science and Technology, Taipa, Macau, China.

[b] Tianjin Key Laboratory of Advanced Functional Porous Materials, Institute for New Energy Materials & Low-Carbon Technologies, School of Materials Science and Engineering, Tianjin University of Technology, 391 West Binshui Road, Xiqing District, Tianjin 300384, China

[c] Faculty of Information, Macau University of Science and Technology, Taipa, Macau, China.

[d] Multi-scale Porous Materials Center, Institute of Advanced Interdisciplinary Studies, School of Chemistry and Chemical Engineering, Chongqing University, Chongqing 400044, China

[e] Advanced Membranes and Porous Materials Center, King Abdullah University of Science and Technology, Thuwal 23955-6900, Kingdom of Saudi Arabia

Correspondence

E-mail: wzhang@must.edu.mo, jianfeng.huang@cqu.edu.cn, yfzhao@tjut.edu.cn;

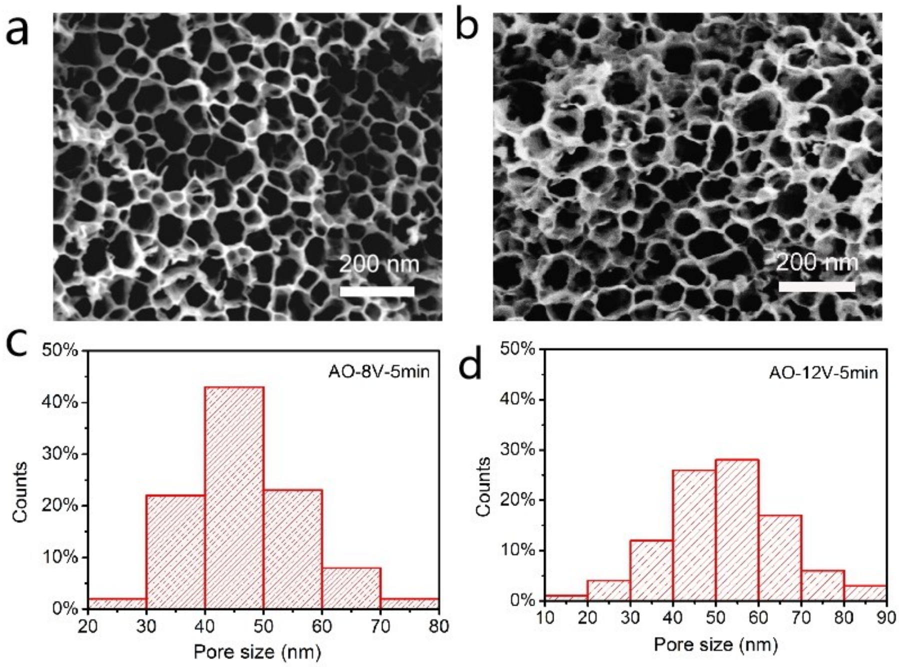

Fig. S1 (a, b) SEM images taken from the surface of SnO_2-AO_8 and SnO_2-AO_{12}, and (c, d) their corresponding pore size distribution graphs

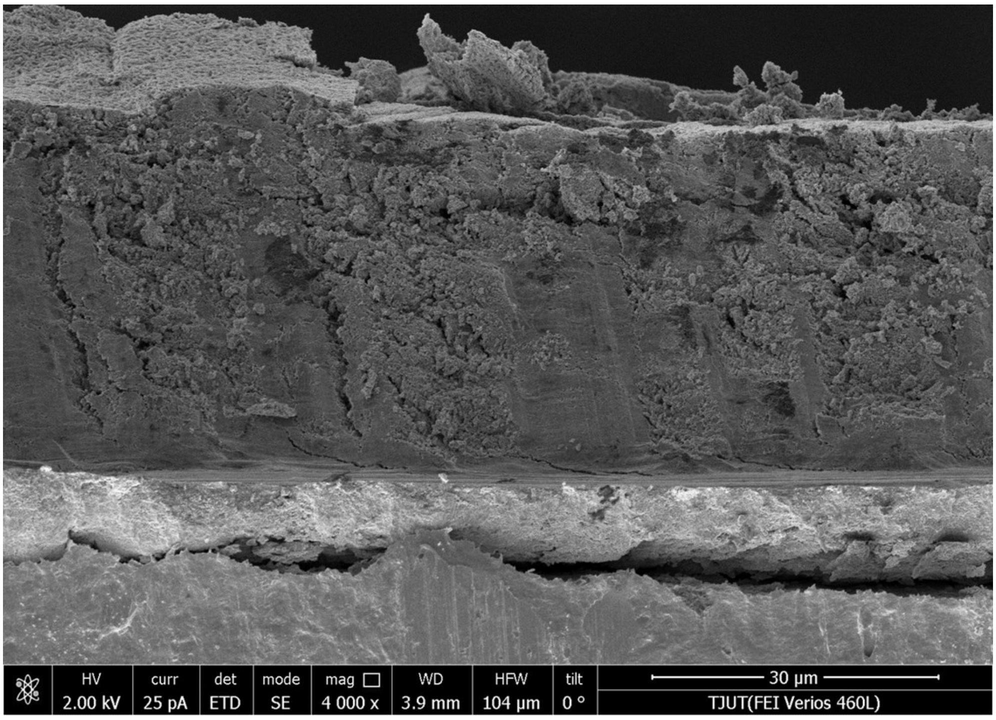

Fig. S2 SEM image taken from the cross-section of SnO_2-AO_{10}.

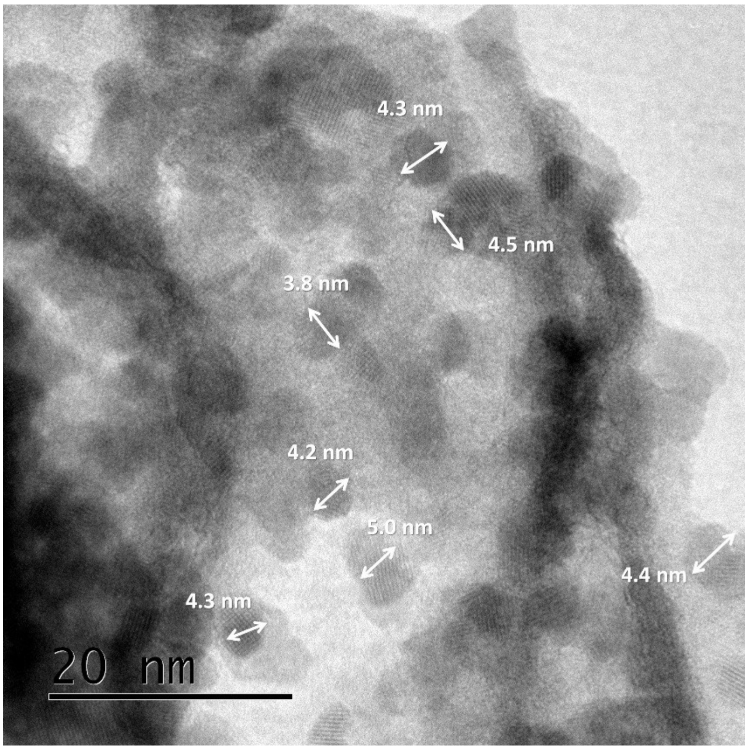

Fig. S3 High-resolution TEM image of SnO_2-AO_{10} nanostructures.

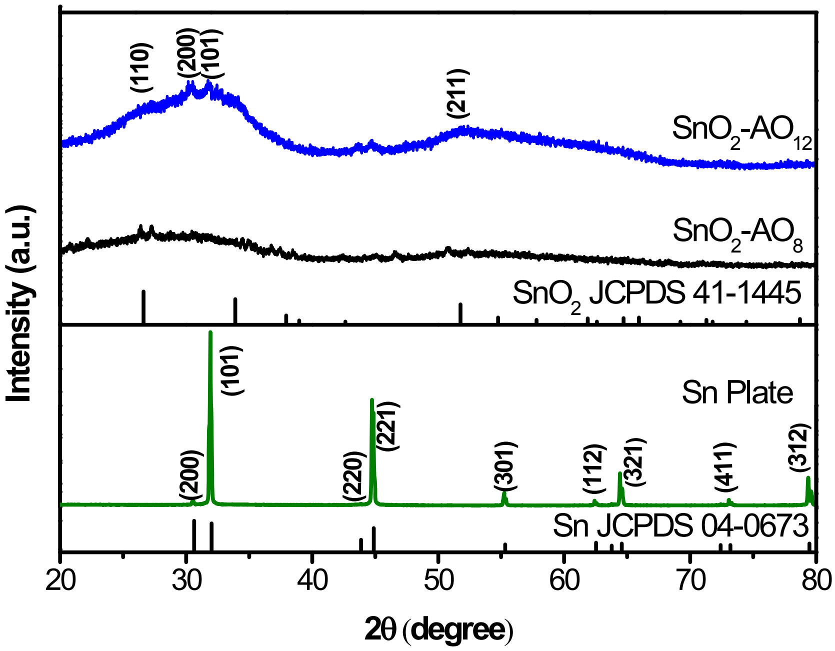

Fig. S4 XRD patterns of Sn foil, SnO_2-AO_8 and SnO_2-AO_{12} nanostructures.

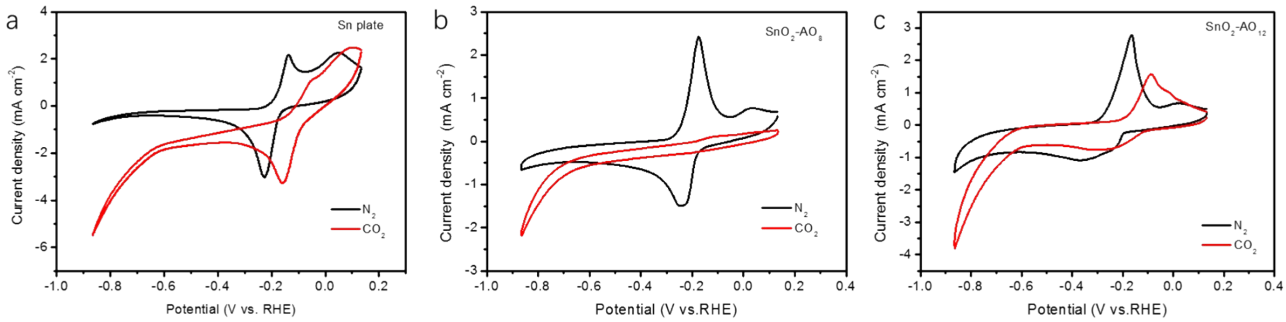

Fig. S5 Polarization curves obtained on (a) Sn plate, (b) SnO_2-AO_8, and (c) SnO_2-AO_{12} in N_2 and CO_2 saturated 0.5 M $KHCO_3$ solution with a scan rate of 50 mV s^{-1}.

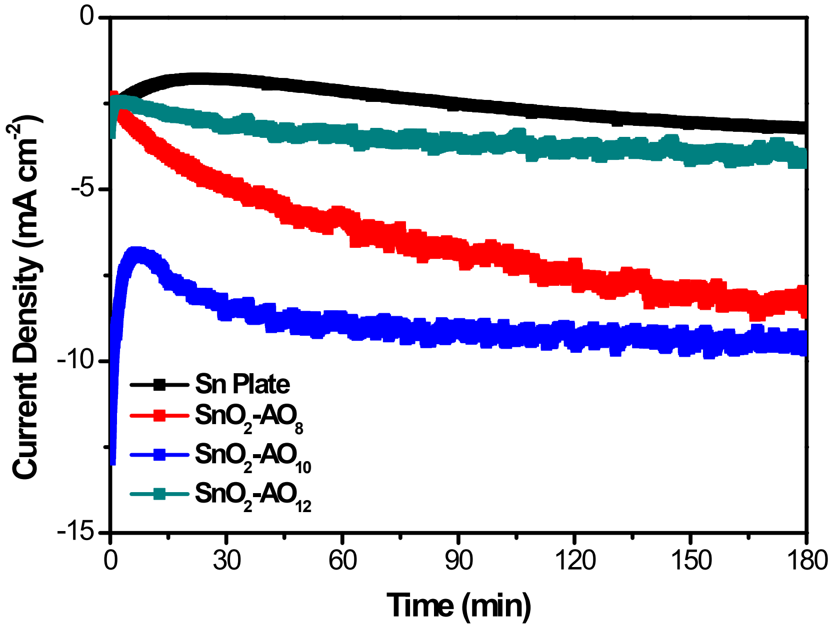

Fig. S6 Current density curves of samples recorded at -0.8 V vs. RHE in 0.5 M $KHCO_3$ with the CO_2 flow rate of 2 mL min^{-1}.

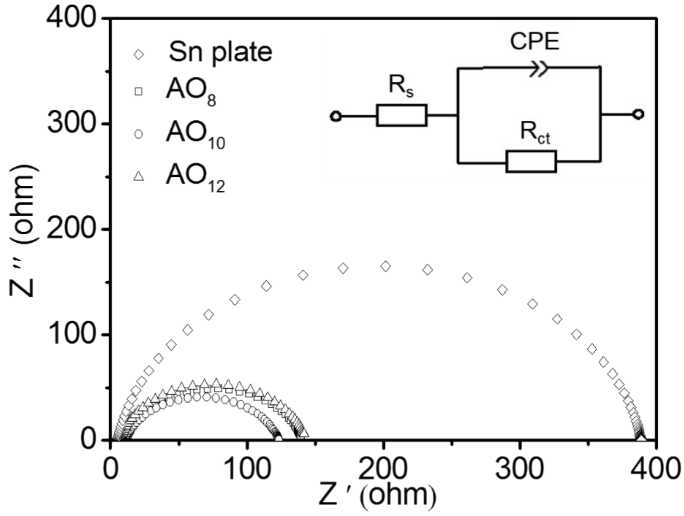

Fig. S7 Electrochemical Impedance Spectroscopy (EIS) analysis SnO_2-AO_8, SnO_2-AO_{10} and SnO_2-AO_{12} electrode in CO_2 saturated 0.5 M $KHCO_3$ solution. The inset is an equivalent circuit diagram for fitting the Nyquist plot. Note: the diameter of the semicircle for SnO_2-AO_{10} is smaller than that of both SnO_2-AO_8 and SnO_2-AO_{12}, signifying that SnO_2-AO_{10} exhibits the smallest charge-transfer resistance (R_{ct}). It is well accepted that the crystallinity of an electroactive material governs its electrical conductivity, which in turn affects significantly its electrocatalytic performance. Consequently, the lower activity of the other two SnO_2 nanostructures (i.e., SnO_2-AO_8 and SnO_2-AO_{12}) might be due to their poorer crystallinity (cf. **Fig.3d** & **Fig. S4**) which limits the electrical conductivity.

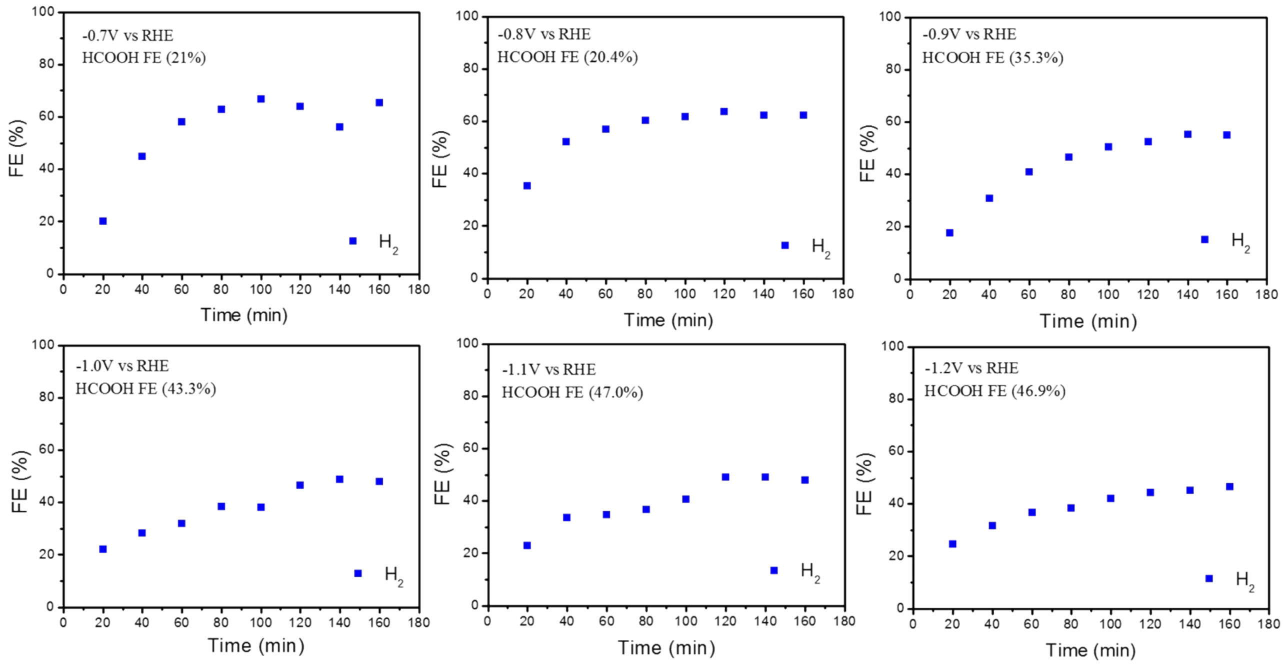

Fig. S8 H_2, CO, and HCOOH FE as a function of electrolysis time on Sn plate electrode at the potential from -0.7 to -1.2 V vs. RHE.

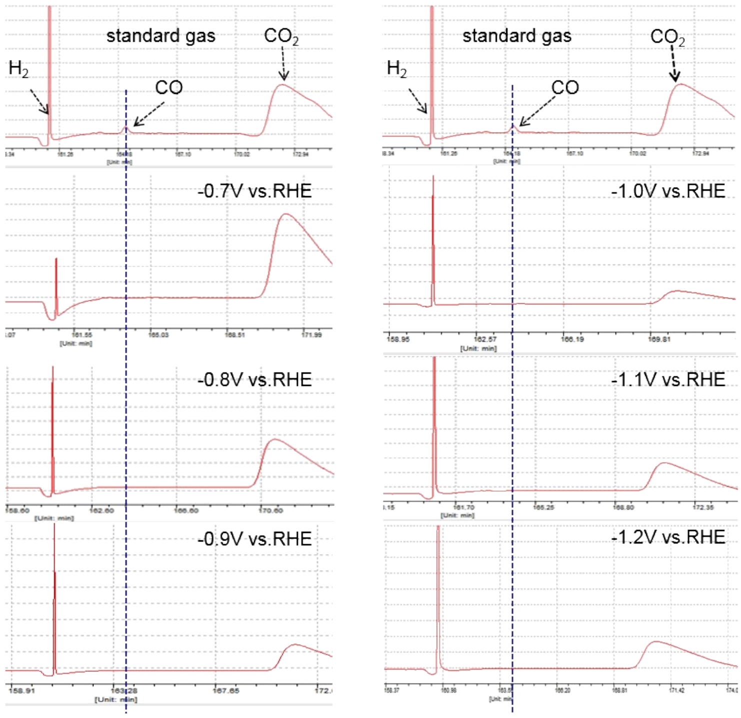

Fig. S9 GC Spectra of products detected on Sn plate at different potentials.

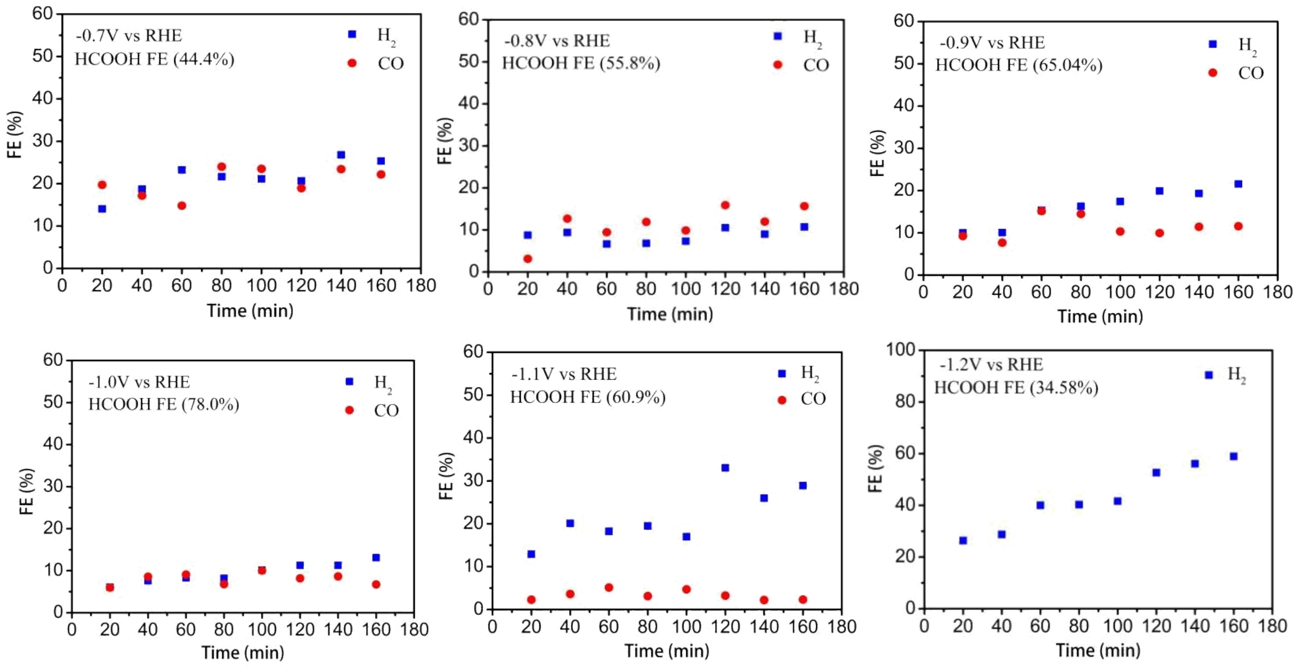

Fig. S10 H_2, CO, and HCOOH FE as a function of electrolysis time on SnO_2-AO_8 electrode at the potential from -0.7 to -1.2 V vs. RHE.

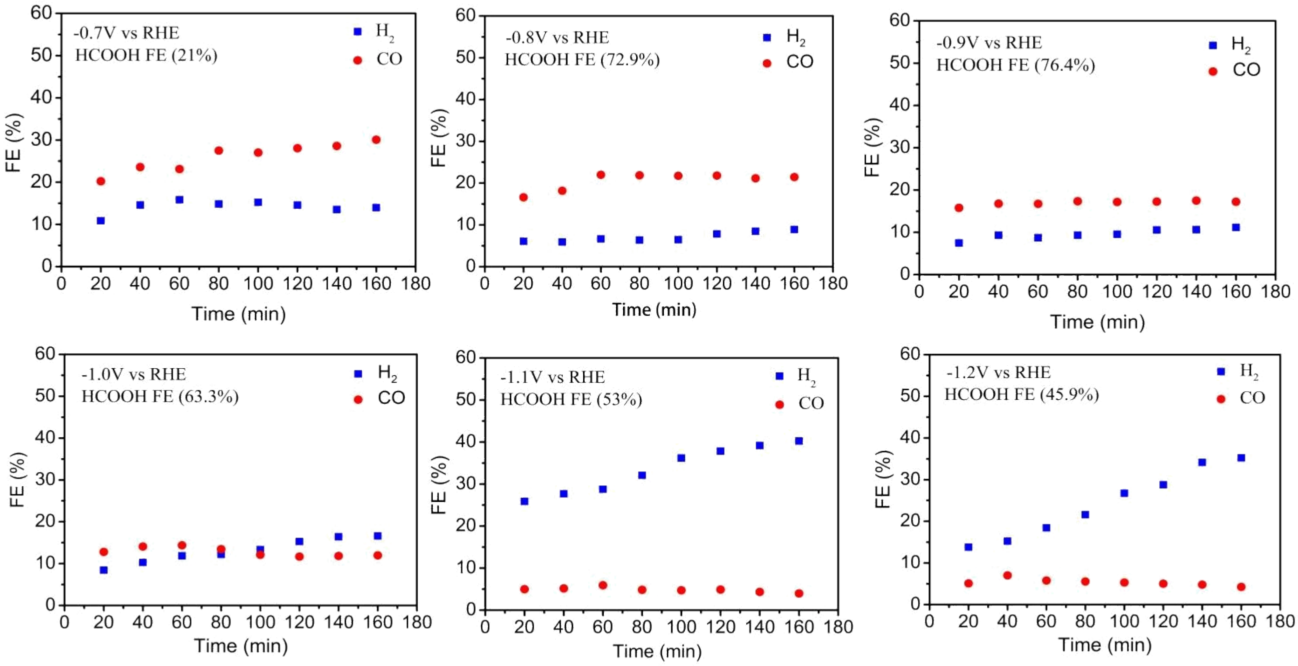

Fig. S11 H_2, CO, and HCOOH FE as a function of electrolysis time on SnO_2-AO_{10} electrode at the potential from -0.7 to -1.2 V vs. RHE.

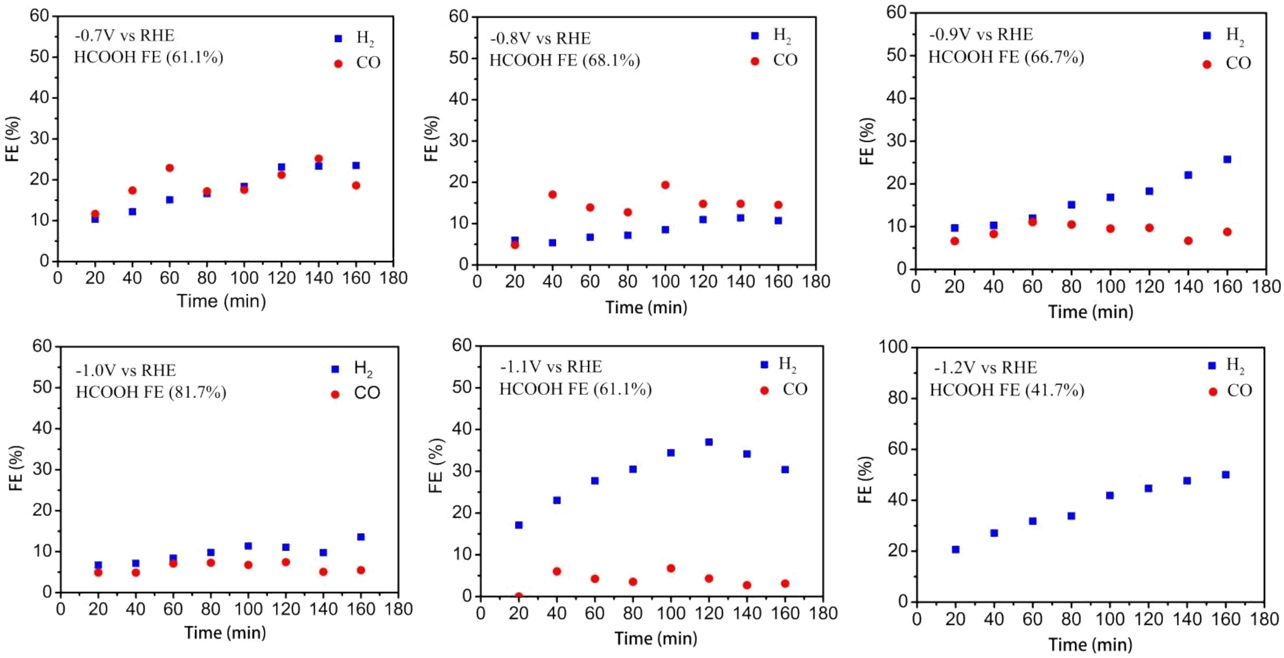

Fig. S12 H_2, CO, and HCOOH FE as a function of electrolysis time on SnO_2-AO_{12} electrode at the potential from -0.7 to -1.2 V vs. RHE.

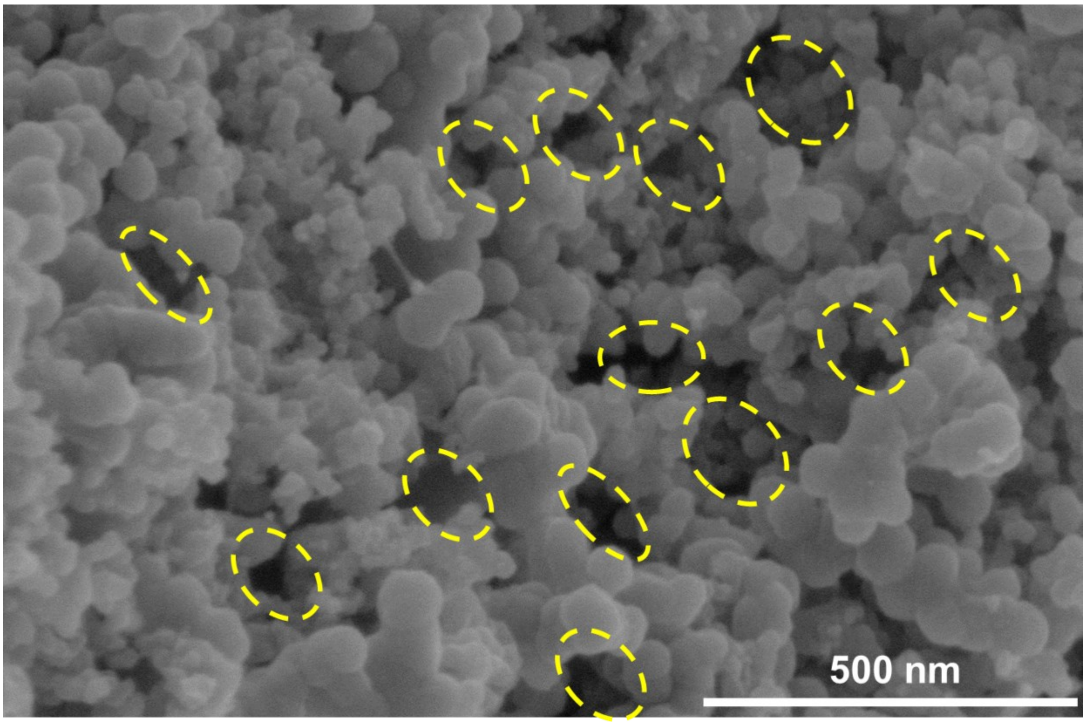

Fig. S13 SEM image of SnO_2-AO_{10} after CO_2RR at -0.8 V vs. RHE for 180 min. The yellow ellipses indicate the presence of macropores.

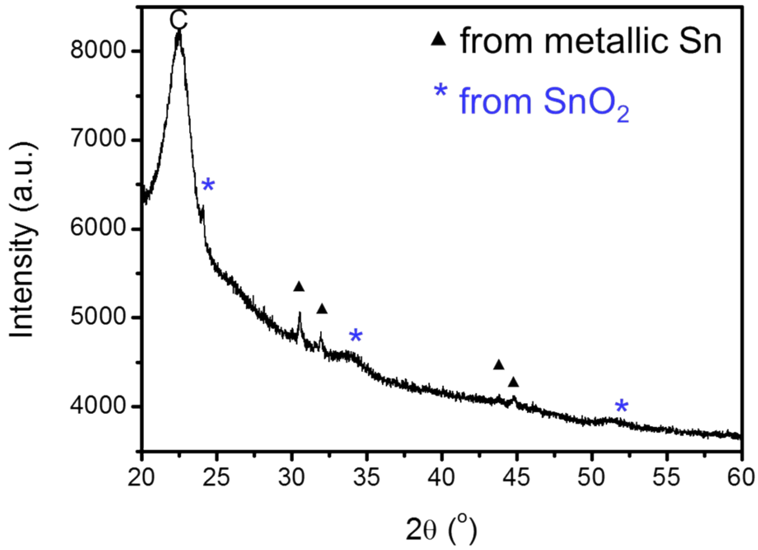

Fig. S14 XRD patterns of SnO_2-AO_{10} after CO_2RR under -0.8 V (vs RHE) for 180 min. Signals of both metallic Sn and SnO_2 were detected. The weak intensity is due to the scarcity of the sample that was collected after reaction. The strong peak at 22° arises from the carbon black.

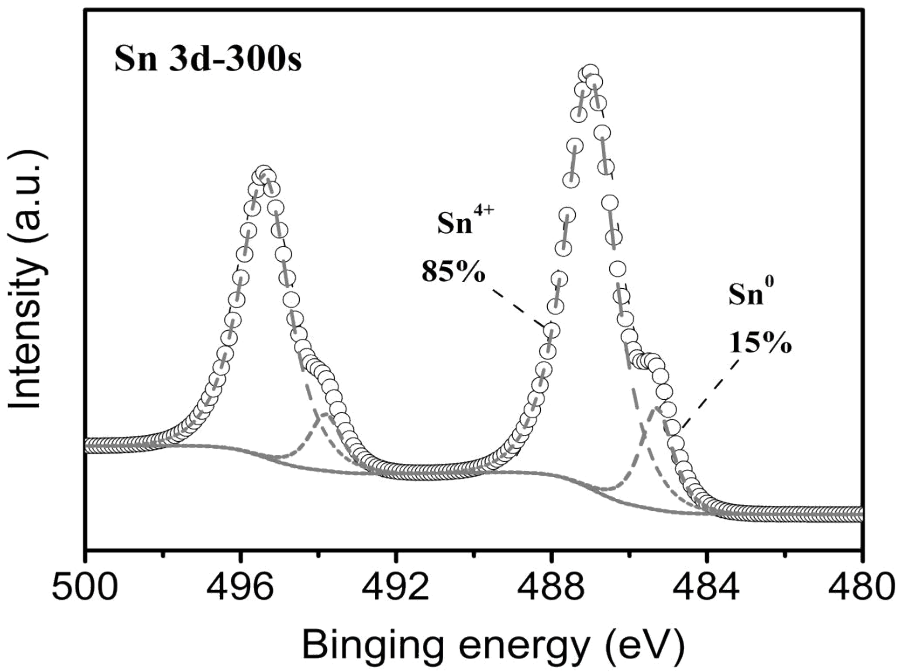

Fig. S15 Depth XPS analysis (sputtering rate: 0.72 nm/s, sputtering time: 300 s) of SnO_2-AO_{10} after CO_2RR at -0.8 V vs. RHE for 180 min.

Table S1. Comparison of working potentials and FEs for CO, HCOOH and C1 of Sn-based CO_2RR from the literature and this work.

Sn-based Catalysts	**Electrolyte**	**Potential** [a] (V vs. RHE)	**FE max (%)**			**Reference**
			CO	HCOOH	CO+HCOOH	
SnO_2@Carbon	0.1M $NaHCO_3$	-1.19	NA	96.3	NA	1
SnO_2-50	0.5M $KHCO_3$	-0.56V vs.SHE	NA	56	NA	2
Graphene confined Sn quantum sheets	0.1M $NaHCO_3$	-1.16	NA	89	NA	3
Sn-pNW	0.1M $KHCO_3$	-0.8	14	78	92	4
Core/Shell Cu/SnO_2 Structure	0.5M $KHCO_3$	-0.7	93	NA	NA	5
Urchin-like SnO_2	0.5M $KHCO_3$	-1.4	NA	62	NA	6
Mesoporous -SnO_2	0.1M $KHCO_3$	-0.8	38	~40	~80	7
SnO/C	0.5M $KHCO_3$	-0.66	37	NA	NA	8
Tin oxide NP	0.5 mol dm^{-3}	-0.4	NA	70	NA	9
porous $Sn_{0.29}In_{0.71}$	0.1M $NaHCO_3$	-1.0	~13	59.2	~72	10
Sn/SnO_2 porous hollow fiber	0.1M $KHCO_3$	-0.95	~10	82.1	93	11
SnO_x/AgO_x	0.1 M KHCO 3	-0.8	~60	21.1	95	12
CuSn-NW Air	0.5M $KHCO_3$	-1.0	NA	90.2	NA	13
CuSn-NW Air	0.5M $KHCO_3$	-0.9	NA	81.2	NA	13
SnO_2-AO_8	0.5M$KHCO_3$	-0.8	15.7	55.8	71.5	This work
SnO_2-AO_8	0.5M$KHCO_3$	-1.0	6	78	84	This work
SnO_2-AO_{10}	0.5M$KHCO_3$	-0.8	22	72.9	**~95**	This work
SnO_2-AO_{10}	0.5M$KHCO_3$	-0.9	15	76.4	91.4	This work
SnO_2-AO_{12}	0.5M$KHCO_3$	-0.8	15.6	68.1	83.7	This work
SnO_2-AO_{12}	0.5M$KHCO_3$	-1.0	5	**81.7**	87	This work

Note: The potentials were converted to RHE scale based on the equation, E(RHE) = E(Ag/AgCl) + 0.0591×pH + 0.210 V or E(RHE) = E(SCE) + 0.0591×pH + 0.242 V by assuming the pH of CO_2-saturated 0.5 M and 0.1 M $NaHCO_3$ or $KHCO_3$ is 7.2 and 6.8, respectively. [a] the best value reported.

Reference in Table S1:

1. Zhang, S.; Kang, P.; Meyer, T.J. Nanostructured Tin Catalysts for Selective Electrochemical Reduction of Carbon Dioxide to Formate. *J. Am. Chem. Soc.* **2014**, 136, 1734-1737.

2. Fu, Y.; Li, Y.; Zhang, X.; Liu, Y.; Zhou, X.; Qiao, J. Electrochemical coreduction to formic acid on crystalline snonanosphere catalyst with high selectivity and stability. *Chinese. J. Catal.* **2016**,

37, 1081-1088.

3. Lei, F.; Liu, W.; Sun, Y.; Xu, J.; Liu, K.; Liang, L. Metallic tin quantum sheets confined in graphene toward high-efficiency carbon dioxide electroreduction. *Nat. Commun.* **2016**, 7, 12697.

4. Kumar, B.; Atla, V.; Brian, J. P.; Kumari, S.; Nguyen, T. Q. Reduced SnO_2 porous nanowires with a high density of grain boundaries as catalysts for efficient electrochemical CO_2-into-HCOOH conversion. *Angew. Chem. Int. Ed.* **2017**, 56, 3645-3649.

5. Li, Q.; Fu, J.; Zhu, W.; Chen, Z. Tuning Sn-Catalysis for Electrochemical Reduction of CO_2 to CO via the Core/Shell Cu/SnO_2 Structure. *J. Am. Chem. Soc.* **2017**, 139, 4290-4293.

6. Liu, Y.; Fan, M.; Zhang, X.; Zhang, Q.; Guay, D.; Qiao, J. Design and engineering of urchin-like nanostructured SnO_2 catalysts via controlled facial hydrothermal synthesis for efficient electro-reduction of CO_2. *Electrochim. Acta*. **2017**, 248, 123-132.

7. Ge, H.; Gu, Z.; Han, P.; Shen, H. Mesoporous tin oxide for electrocatalytic CO_2 reduction. *J. Colloid. Interf. Sci*. **2018**, 531, 564-569.

8. Gu, J.; Héroguel, F.; Luterbacher, J.; Hu, X. Densely packed, ultra-small SnO nanoparticles for enhanced activity and selectivity in electrochemical CO_2 reduction. *Angew. Chem. Int. Ed*. **2018**, 57, 2943-2947.

9. Dutta, A.; Kuzume, A.; Kaliginedi, V. Probing the chemical state of tin oxide NP catalysts during CO_2 electroreduction: A complementary operando approach. *Nano Energy* **2018**, 53, 828-840.

10. Hyenki, K.; Hyunju, L.; Taeho, L. Facile fabrication of porous Sn-based catalysts for electrochemical CO_2, reduction to HCOOH and syngas. *J. Ind. Eng. Chem*. **2018**, 66, 248-253.

11. Hu, H.; Gui, L.; Zhou, W.; Sun, J. Partially reduced Sn/SnO_2 porous hollow fiber: A highly selective, efficient and robust electrocatalyst towards carbon dioxide reduction. *Electrochim. Acta.* **2018**, 285, 70-77.

12. Choi, Y.W.; Scholten, F.; Sinev I.; Cuenya, B.R. Enhanced Stability and CO/Formate Selectivity of Plasma-Treated SnO_x/AgO_x Catalysts during CO_2 Electroreduction. *J. Am. Chem. Soc*. **2019**, 141, 5261-5266.

13. Wang, J.; Ji, Y.; Shao, Q.; Yin, R.; Guo, J.; Li, Y.; Huang, X. Phase and structure modulating of bimetallic CuSn nanowires boosts electrocatalytic conversion of CO_2. *Nano Energy* **2019**, 59, 138-145.